

SIMULATION OF THE MAGNETIC FIELD OF A SUPER CONDUCTING SOLENOID IN SCOPE OF THE MUON EDM EXPERIMENT AT PSI

Author:

Philipp Pestlin

ppestlin@student.ethz.ch

Advisors:

Prof. Dr. Klaus Kirch

Dr. Chavdar Dutsov

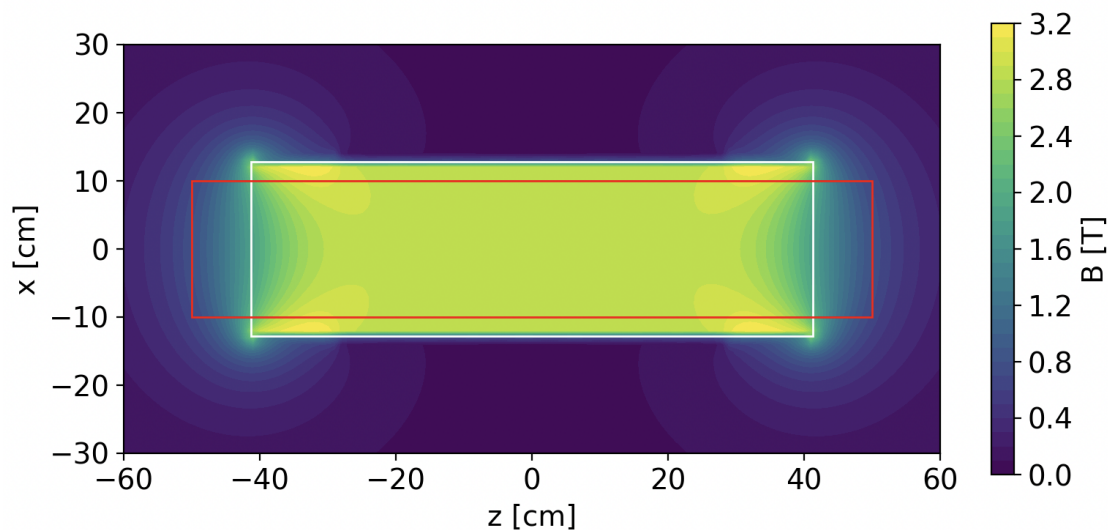
Dr. Philipp Schmidt-Wellenburg

Bachelor Thesis at PSI

Vladimir-Prelog-Weg 2, 8093 Zürich, Switzerland

Interdisciplinary Sciences B. Sc.

May 1, 2023



Contents

1	Introduction	2
2	Theory	3
2.1	Magnetic field inside a solenoid	3
2.2	Calculation of uncertainties	5
3	Experiment	6
3.1	Measurements	6
3.2	Python implementation	7
4	Results and Discussion	8
4.1	Uncertainty parameters	8
4.2	An overview	9
4.3	Coil parameters	13
4.4	Systematic error patterns	14
4.5	Direct comparison	15
4.6	Information transfer for tracking simulations	16
5	Conclusion and Outlook	17
	Appendices	19

1 Introduction

In the course of this thesis I developed a computer program that approximates the magnetic field of a superconducting solenoid using a set of measured field data points. The main purpose of the software is to generate field maps with sub-millimeter resolution in formats that are necessary in Geant4-based programs for Monte Carlo particle transport.

The work is conducted as part of the Muon EDM experiment which is ongoing at the Paul Scherrer Institute (PSI). The main goal of the experiment is to search for an electric dipole moment (EDM) of the muon. The existence of a non-zero EDM of a fundamental particle such as the muon is a clear sign of Charge-Parity symmetry (CP) violation. The Standard Model of particle physics is successful at explaining the overwhelming majority of particle physics experimental results. However, while it allows for CP violating processes they are insufficient at accounting for the observable imbalance between matter and antimatter. The current experimental upper limit of the muon EDM (muEDM) is set at $|d_\mu| < 1.8 \times 10^{-19} e \cdot \text{cm}$ (95% C.L.) [1] while the PSI experiment aims to reach a sensitivity of $3 \times 10^{-21} e \cdot \text{cm}$ in the first part and later possibly a sensitivity of $6 \times 10^{-23} e \cdot \text{cm}$ [2]. Measuring an EDM of the muon at this level would clearly deviate from the prediction within the standard model by many orders of magnitude as the predicted muon EDM is at least $|d_\mu| < 1.1 \times 10^{-29} e \cdot \text{cm}$ (90% C.L.) [3, 4].

In order to measure the EDM of the muon the collaborators will use the frozen-spin technique [5] where the muons are kept inside compact solenoid. In order to store the muons into stable orbit within a weakly focusing field at the center of the solenoid a superconducting injection line and a magnetic pulse-kick will be used. In the storage ring the spin of the muon will precess due to the coupling of the anomalous magnetic moment with the longitudinal magnetic field of the solenoid. In the frozen-spin experiment two cylindrical electrodes will provide a radial electrical field in order to achieve the frozen-spin condition [6], where, for an appropriate value of the electric field, the anomalous precession can be negated.

Due to the necessary precision and the fact that the experiment is conducted within the solenoid, it is of high interest to have precise magnetic field maps for the area in and around the solenoid in order to run Monte Carlo simulations on muons entering the setup. The code I developed in Python is capable of deriving such field maps from field data measured inside a solenoid and offers the capability to include additional devices introduced in the future.

2 Theory

2.1 Magnetic field inside a solenoid

Biot-Savart's law is an equation within electromagnetism that describes the magnetic field generated by a constant electric current. It is a vector equation that gives the magnetic field in the three spacial directions. The magnetic field dB from a wire element with infinitesimal length is then given by:

$$dB = \frac{\mu_0}{4\pi} \frac{Id\hat{l} \times \hat{r}}{|r|^2}, \quad (1)$$

where μ_0 is the vacuum permeability, I is the current running through the wire element $d\hat{l}$, r is the vector between the wire element and the point of interest in space and \hat{r} is its unit vector.

For complex systems such as a solenoid there are no exact analytical solutions for the B -field. Instead, one can choose between different methods to reduce the problem into smaller sub-problems for which one knows the solution. Using the principle of superposition, one can later obtain the magnetic field at any position.

One possible approach is to replace a complex coil, such as a solenoid, with many straight line wire pieces. The vector describing such a wire element as well as the point in space always form a plane which simplifies the cross product as $d\hat{l} \times \hat{r} = dx \sin \theta \hat{k}$ with $dx = |d\hat{l}|$, θ the angle between both vectors and \hat{k} the normal vector to the plane. From simple right angular triangle rules we can further substitute with $r = a/\sin \theta = a \csc \theta$ and $x = a/\tan \theta \implies dx = -a \csc^2 \theta d\theta$ where a is the distance between the point and the line containing the wire. This then gives:

$$dB = \frac{\mu_0 I}{4\pi} \frac{-a \csc^2 \theta \sin \theta d\theta}{(a \csc \theta)^2} \hat{k} = -\frac{\mu_0 I}{4\pi} \frac{\sin \theta d\theta}{a} \hat{k}. \quad (2)$$

Integrating over theta from the start ($\theta = \pi - \theta_1$) to the end ($\theta = \theta_2$) of the wire then gives:

$$B = -\frac{\mu_0 I}{4\pi a} \int_{\pi-\theta_1}^{\theta_2} \sin \theta d\theta = \frac{\mu_0 I}{4\pi a} (\cos \theta_2 + \cos \theta_1). \quad (3)$$

The field therefore only depends on the angles between the wire and r at both ends of the wire as well as the distance a which we can always determine. For cases where the condition $r \gg l$ (l being the length of a straight piece) is fulfilled we can also use the approximation $\frac{dr}{dx} = 0$ which will give very similar results. Considering a solenoid modelled using thousands of small pieces where only a small number of pieces does not fulfil the condition the model gives a good approximation. Then we can simply replace the small

wire piece $d\hat{l}$ in the initial equation with \hat{l} and no further integration is necessary. Decreasing the size of l increases the accuracy of both approaches and also lowers the difference between the analytical solution and the approximation.

To create a solenoid from straight pieces of wire we need to choose a finite length leading to some approximation. By using 20 to 60 pieces of wire for each winding we are able to reach very similar results. Using more pieces is not feasible for the magnets investigated over the course of this thesis as it would lead to much larger computing times. The effect of using smaller pieces can also be interpreted as increasing the effective radius of each layer. For points which are not close to the wire, an increase in the amount of pieces will therefore only have a rescaling of the radius as an effect. Additionally we also need to decrease the amount of windings we are using, again to save on computing time. Instead of 100 windings each carrying 75 A we only use one winding carrying 7500 A. Simulations with the initial and the rescaled number of windings show identical results. This can be explained as the rescaling conserves the symmetry in good approximation and the current density stays identical which is the property we can determine with our simulation anyways.

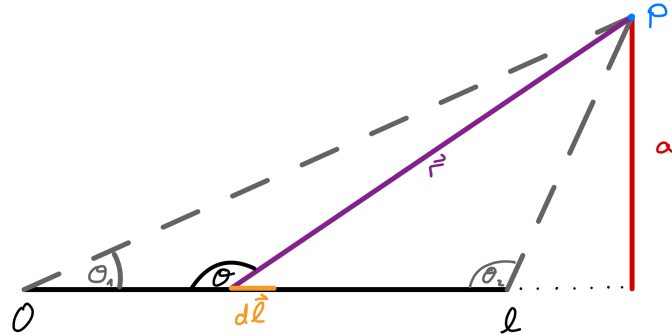


Figure 1: Sketch of a the geometry for a wire of length l which field is to be determined at the point p .

Other approaches to model the solenoid may consider a finite and continuous solenoid. Continuous means that the system is not modelled using many individual coils but rather as a plate of conductive material carrying a charge density. Here the vector potential \vec{A} can be used to find the magnetic field $\vec{B} = \nabla \times \vec{A}$. Eventually we did not consider this approach as it would be relatively calculation heavy and therefore unsuited for large amounts of repeated simulations. An interested reader can still find a detailed derivation under [7].

After implementing the calculation of the magnetic field at a specific point we are now interested in optimising our initial calculations to an optimal configuration. In order to do so using numerical methods we need to determine an expression for the residues while considering possible errors which could have effected the quality of the data at hand. The

derivations and considerations for these will be discussed in the following section.

2.2 Calculation of uncertainties

When finding the uncertainty of a specific measurement it is important consider all possible contributions. The overall variance is given by them sum of variances from all sources, assuming the individual variances are not correlated:

$$\sigma^2 = \sum_n \sigma_n^2. \quad (4)$$

One uncertainty when measuring a magnetic field will always arise from the discrete values displayed by the measurement device. For a digital device with a finite number of digits the real value is within plus and minus half of a division. For the uncertainty of the shown value one can assume a uniform distribution within these bounds where the standard deviation of a uniform distribution is given by $(b - a)/\sqrt{12}$ where a and b are the boundaries of one division.

Furthermore, there is some uncertainty in the z-position at which the measurement was taken, leading to a level of uncertainty in the field. The uncertainty directly depends on the gradient of the field around the point of measurement. This reasoning can be best understood by looking at two examples: First, we consider a constant field, therefore $B(z) = b$. If we have some uncertainty in z this will not change the measured value of B as $\text{grad}(B) = 0$. If we instead consider $B(z) = bz$ a change in z : Δz will change the field to $B(z + \Delta z) = b(z + \Delta z)$. The larger b the more significant is the change in $B(z)$ as the change in field is given by $\text{grad}(B) = b$. Now assuming a constant gradient in the area around the measurement point we find the resulting field uncertainty to be $\sigma_B = \sigma_z \cdot \text{grad}_z(B)$. For data processing it can be better to find a value for σ_B in some area and derive σ_z from this for any further evaluation. For an area where no significant gradient is present, one may still be able to observe an error directly from the measurement data. This will then give us a constant measurement uncertainty $\sigma_{\text{measurement}}$. The overall uncertainty is the given by the following:

$$\sigma_i = \sqrt{(\sigma_z \cdot \text{grad}_z(B_i))^2 + \sigma_{\text{measurement}}^2 + \sigma_{\text{display}}^2} \quad (5)$$

Additionally to these, measured data may be object to calibration errors which will be the same across all measurements. For this project we do not consider such errors as we are interested in the topology of the space and constant or linear offsets do not change these characteristics significantly.

When performing numerical optimisations uncertainties are important in order to balance

out the residues. For any field optimisations a residue is defined as the sum of the difference between the measured field (B^m) and the simulated field (B^s) at position i . The vector of all residuals is known as the residual vector. To incorporate the weight of the error into the optimisation we divide by the uncertainty. The chosen numerical method then minimises the sum of squares of all residues (S) is minimised.

$$R_i = \left| \frac{B_i^m - B_i^s}{\sigma_i} \right| , \quad \vec{R} = \begin{pmatrix} R_0 \\ R_1 \\ R_2 \\ \dots \end{pmatrix} , \quad S = \vec{R} \cdot \vec{R} \quad (6)$$

3 Experiment

3.1 Measurements

Throughout the project we have been working with two superconducting magnets called *PSC*- and *Ben*-magnet. While I participated in the measurements of the Ben-Magnet, the data for the PSC was measured by the group prior to this thesis and provided to me by my supervisor. The casing of the *PSC*-magnet has a length of 1 m with a bore radius of 10 cm while the *Ben*-magnet has a length of 65.4 cm and a bore radius of 15 cm.

To acquire data of the magnetic field inside both magnets we first fixated a straight plastic tube inside the magnet using wooden plates mounted to the edges of the magnet. For the *PSC*-magnet we were able to use multiple wooden plates with holes at different radii which allowed us to take measurements along several longitudinal lines inside the magnet. For the *Ben*-magnet we were not able to use the same wooden plates due to different mounting possibilities on the case of the magnet. We were therefore only able to measure data on the centre line and the outermost radius of the magnet. For measurements of both magnets we used a 3-axis LakeShore 460 gaussmeter [8]. It features a five digits resolution with a 0.1% accuracy and is able to measure up to three tesla. The probe of the gaussmeter was pushed along an inserted plastic tube. The axis along the magnet is referred to as the z-axis while the bore surface gives the xy-plane. The x and y orientation is kept throughout all measurement using a spirit level within 0.6 mrad.

When taking the measurements we are either able to push the probe by 10 ± 0.1 cm and fixate it again, or take the probe out of the tube and adjust it by 2 cm. As we were able to take measurements at many different radii of the *PSC*-magnet we were able to generate a large amount of data only by pushing the rod by 10 cm and the second method was only used in smaller quantity and at important radii (0 cm, 30 cm, 33 cm). For the *Ben*-magnet this was different due to very limited amount of radii and we therefore measured every

2 cm. This gave us a total data set of 584 points for the *PSC*-magnet and 131 data points for the *Ben*-magnet. The entire data set can be found in the appendices. It is important to mention that the field of the Ben magnet went beyond the gauge limit of the measurement probe. We therefore performed the measurement at 2.8 T and rescaled the data linearly to 2.9 T.

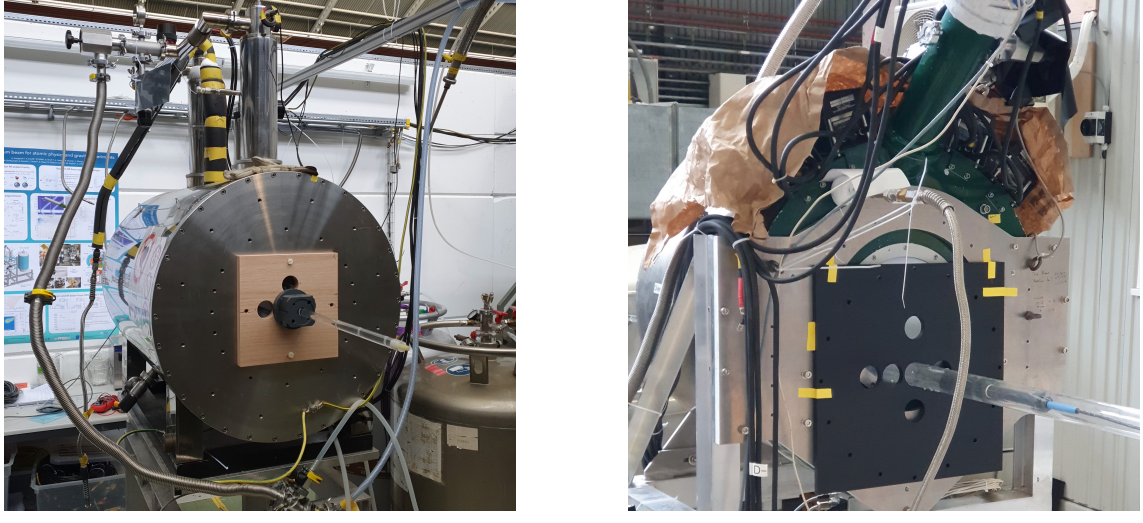


Figure 2: Pictures of the two magnets at the time of the measurements. Clearly visible is the plastic tube going through the bore of both magnets, containing the probe.

3.2 Python implementation

To simulate a magnet and its field on a computer we started off by using a python package called **Biot-savart** [9] which gave the basic structure and idea on how to create coils and numerically calculate the field at points inside the magnet. Throughout the project the package showed to be ill-fitting for the many demands we had for the code.

Be it the input data structure as we needed to calculate the field at specific points and not in a grid or the demand on hardware components due to chosen implementation by the creator of the package. Thus, we were forced to optimize and rewrite all parts of the code. Finally, no original functions are used in our end product.

The code takes all parameters regarding the magnet (radius of the coils, number of windings, length of the magnet, potential offsets to the coordinate system of the measurements etc.) as an input and creates a coil from these. The coils consist of many straight line pieces, each provided with a current. Then we can use Biot Savart's law to calculate the magnetic field at any point in space from each individual piece (using equation 3). Finally, we use the **minimize** function provided with the python package **lmfit** [10] to perform numerical optimisations on the parameters of the coil(s) by minimising the residues between

the field and the calculated values. The entire code can be found in the appendices.

A schematic of the coil created to simulate the magnetic field is shown in figure 3. The main solenoid is shown in blue while the two end coils are coloured in red. For visualisation purposes the amount of windings is strongly reduced compared to the amount used for simulations. Similarly, only one layer of wires is shown instead of multiple layers, which would be separated by 1 mm each.

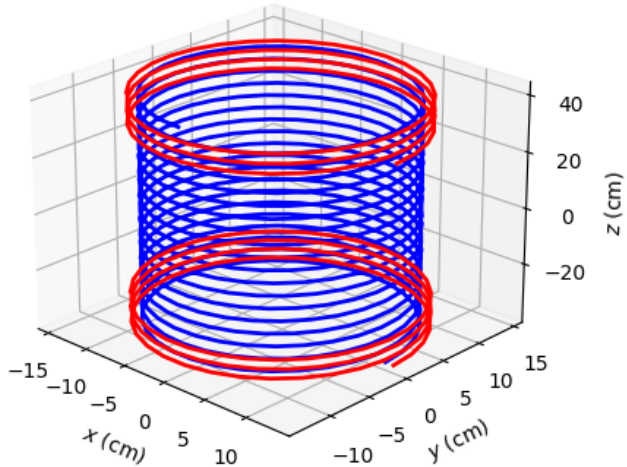


Figure 3: Schematic of a solenoid (blue) with two shimming coils (red).

4 Results and Discussion

4.1 Uncertainty parameters

While we can easily determine the display uncertainty of the 3-channel Gaussmeter as $\sigma_{\text{measurement}} = \frac{0.0001 \text{ T}}{\sqrt{12}}$, we still need to determine σ_z and $\sigma_{\text{measurement}}$ from our data. When measuring the field, we first took a measurement going in one direction, then rotated the probe by 180° and measured again going backwards. From the two measurements of the z component of the field at the same position we took the difference and calculated the standard deviation of this difference. As the effect of the gradient is only relevant at the edges of the solenoid, using values at the edges, in a range of $0.5 \text{ T} - 2.8 \text{ T}$, gives us the uncertainty $\sigma_B \approx 0.003 \text{ T}$ which can slightly vary between different measurement positions by some tenth of a mT. The gradient in this area in a linear approximation is found to be $\text{grad}_z(B_i) \approx 15 \text{ mT/mm}$ giving us the position uncertainty $\sigma_z = \frac{\sigma_B}{\text{grad}_z(B_i)} = 0.2 \text{ mm}$. For the constant uncertainty (measurement uncertainty) we use the same procedure but only consider values which were above 2.8 T as here the field gradient is negligible and we are most interested in this are in terms of the final experiment. We find $\sigma_{\text{measurement}} \approx 0.6 \text{ mT}$

which can again vary on the order of 0.1 mT. While the gradient can differ between the two magnets in principle, we nonetheless assume the PSC-uncertainties for both magnets as these should only depend on the probe and the measurement setup and should therefore be similar. This is also considering the similarity in the field on the edges of both magnets.

4.2 An overview

We will first show general results of the simulations (figure 4) before looking at the findings in more detail. For all plots we included a graph depicting the position in the X and Y plane at which the depicted measurements were taken. The blue circle represents the bore of the magnet.

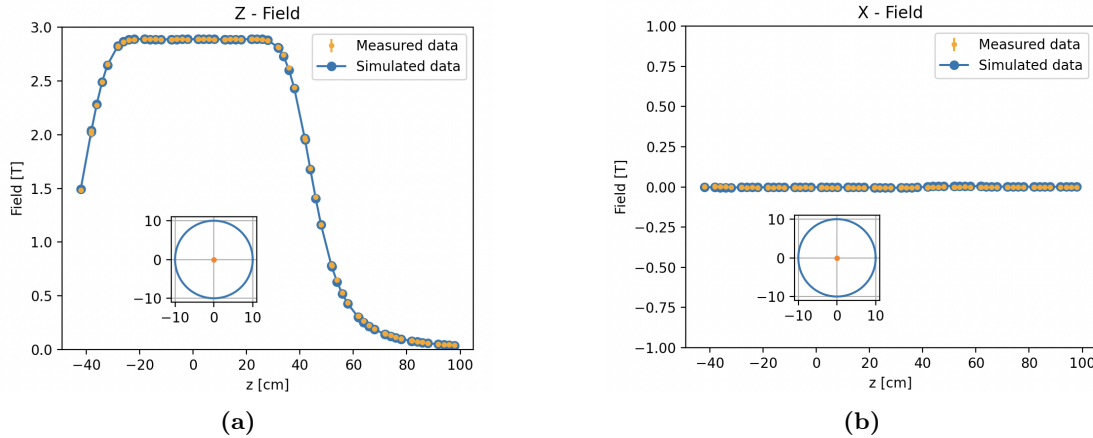


Figure 4: Shown are the X and Z component of the magnetic field vector at position $(0, 0, z)$. In orange we show the data from the measurements and in blue we show the result of our calculation for the respective measurement point. The Y component shows a very similar form as the X component and can be found in the appendices.

Not only do the results of the simulation describe the shape of the measurements but we also see the expected shape on the large scale. The large gradient in the Z field which is present around the edge of the magnet highlights the importance of including a gradient dependent uncertainty. This is shown by the large difference in field strength for consecutive points which are only set apart by 2 cm.

If we look at different measurement points in the x-y plane the shape for the Z component continues to be the very similar while the x and y components show non zero fields. This is especially visible on the edge of the solenoid as the total field starts to curve around the solenoid at this point. We can see this effect best if look at a point on the x or y axis as the effect there will fully go into the x or y component respectively while the other component remains about constant.

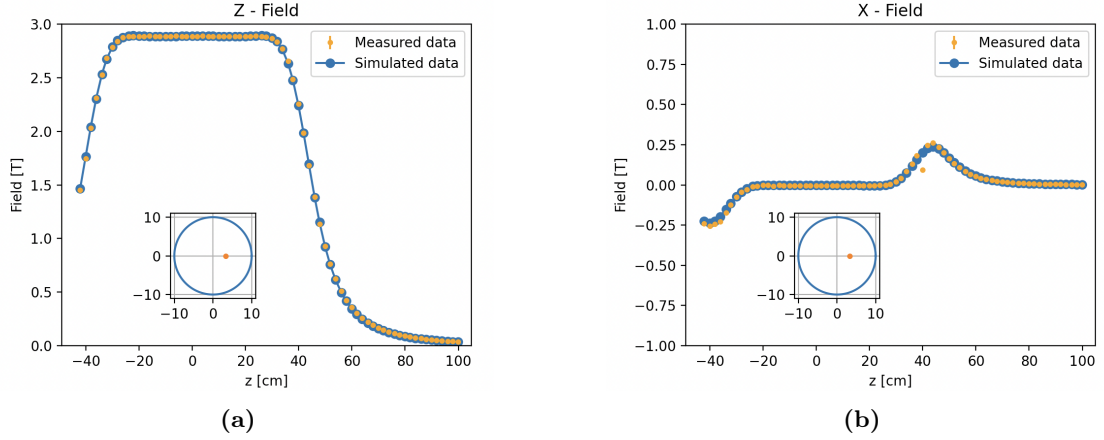


Figure 5: $x = 3.3$ cm field of the PSC-magnet.

While the z component at $x = 3.3$ cm is very similar to what is seen in the center (4a) we can see a clear change in the x component. Around $z = 40$ cm we have the field bending out of the magnet, therefore $B_x > 0$ while around $z = -40$ cm the field bends into the bore, leading to $B - x < 0$.

Next we can use the generated field map to produce contour plots to visualise the field in and around the solenoid. Even at low resolutions of steps every 0.1 T, we can see the effects of the end coils as bumps in the magnetic field are visible on the edges. A large reason for the clear visibility, especially in contrast to figures 4a & 5a, is the fact that we use the absolute value of the field to create the plot. This means that the bumps are largely caused by the extrema seen in the x or y component (see figure 5b).

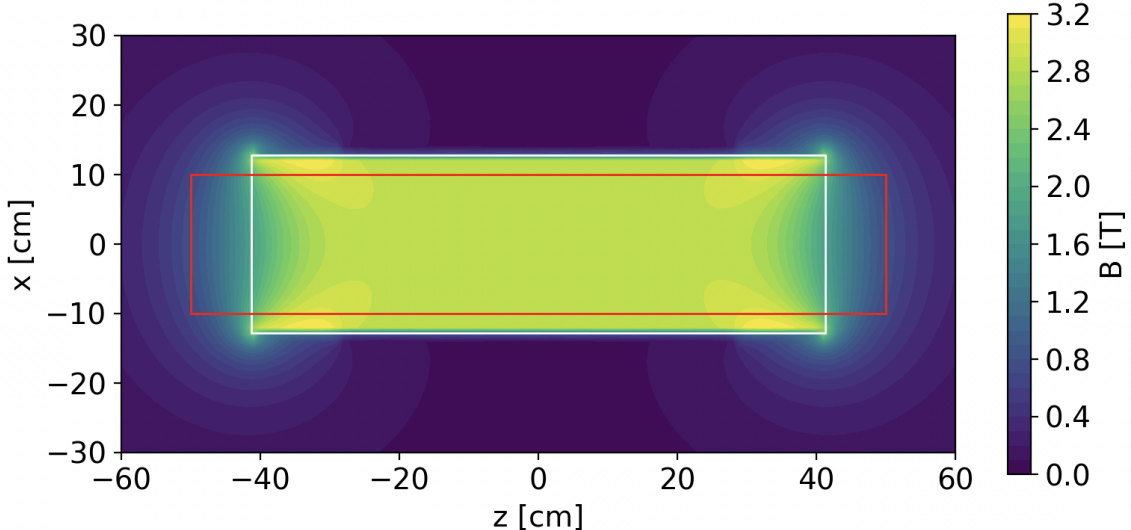


Figure 6: Contour plot showing $|B|$ over the x - z plane at $y = 0$ for the PSC magnet. The red box shows the area in which the bore of the magnet lies while the white box depicts the position of the coils. We can see the relative constant field in the center of the magnet with a steep fall off on the edge.

For the Ben magnet we had initial difficulties due to the limited possibilities of mounting the tube for the probe. This lead to a different offset for the center and the second location relative to the intended placement. To compensate for this we translated the the x and y component into a radial and an angular component as $|B_r| = \sqrt{B_x^2 + B_y^2}$ and $B_\phi = 0$. While in practice the angular component does not necessarily need to be 0, which might be caused by imperfections in the wiring, the assumption is already implied by the symmetry of the generated coil. Instead of rewriting the code we performed the transformation on the input data and treat B_r as B_y . For the sign of B_r we manually looked at the direction of the field and the quadrant it was in.

The simulation for this was performed using a version of the code based on the $r \gg l$ approximation. The results from this fit still shows a good approximation to data but running the fitting algorithm suddenly lead to an unreasonable divergence. For now we were unable to identify the reason for this divergence, especially as the same code converged to the shown results of the PSC magnet. Therefore we were only able to improve the results by adjusting parameters manually to look for better results and could not find a global minima like we did for the PSC magnet (assuming the numerical methods found the actual global minima).

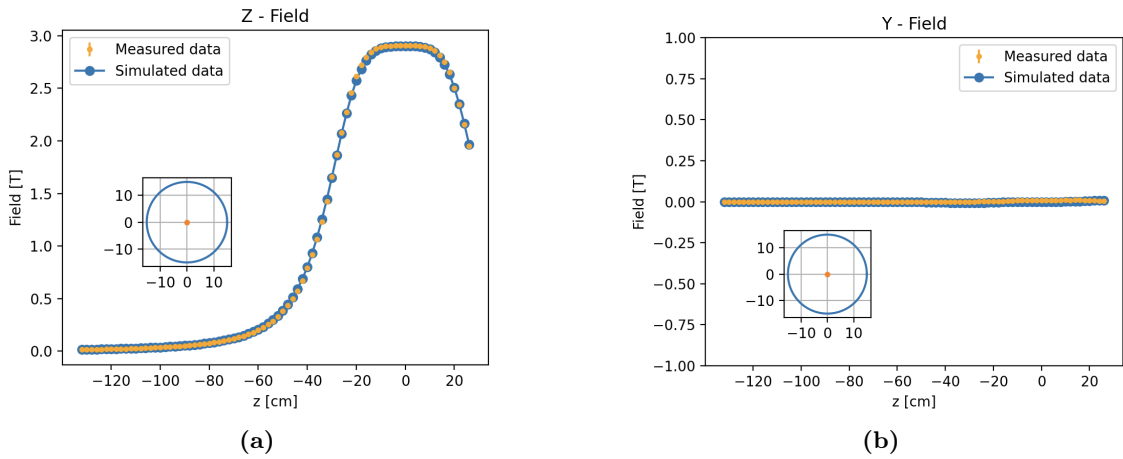


Figure 7: Center field of the Ben magnet. The graph now shows a 15 cm bore radius in adjusting for the magnet.

For the field in the center is the size difference in length compared to the PSC magnet is especially noticeable. The data also seems to fall off in field strength slightly faster than the simulated data but it still seems to be within a reasonable range.

For the second location we had to go to $y = 12.5$ cm as mentioned earlier. This leads to much larger bumps on the edges in comparison to the PSC magnet which in principle features a similar topology in the field but one which is not resulted in a full scale image.

We therefore can not make any comparisons yet but will rather look at the simulated data at the same radius at a later stage.

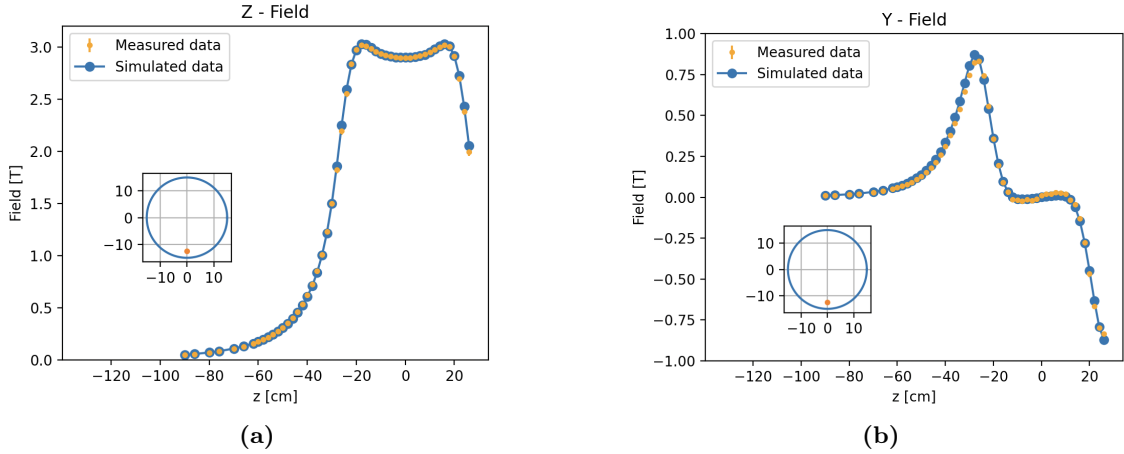


Figure 8: $y = -12.5$ cm field of the Ben magnet.

With this data at $y = -12.5$ cm we already see some clear deviations between measurement and simulated data. The first peak in 8b seems slightly left shifted and also shows a maximum larger than that of the recorded data. For the Z field we can also see some deviations around the edges in a similar way to the field in the center shown in 7.

To understand the course of the field between the very outside and the center of the magnet a bit better we again also show a contour plot for the Ben magnet. While it seems much more dense than the contour plot of the PSC magnet this is largely due to the smaller size leading to no formation of a plateau in magnetic field. This shows that a constant field approximation for the inside of a solenoid is only justified for solenoids of large length.

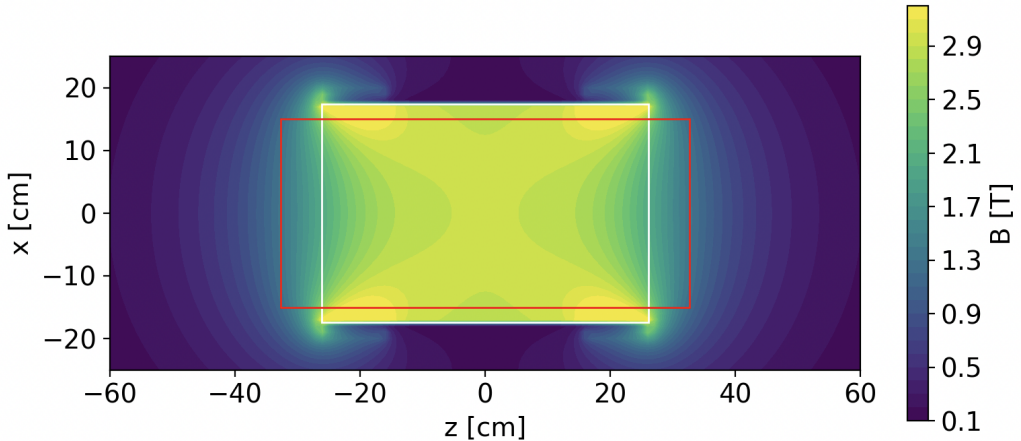


Figure 9: Contour plot showing $|B|$ over the x-z plane at $y = 0$ for the Ben magnet. We again mark the bore with a red rectangle and the coil with a white rectangle. For the field inside the solenoid we can clearly see a typical saddle point shape where going along the x and z axes from the center the field becomes weaker and along the diagonal axes the field becomes stronger.

4.3 Coil parameters

With our python implementation we initialise several parameters which we will show in the following section. The parameters are error prone as they are numerically detected parameters determined from measurement data. As the parameters are strongly correlated it is hard to determine proper errors. Eventually, we also give the results to a certain number of digits but do not name the precise value found by the fitting algorithm.

We will first look at the parameters for the PSC magnet. First of all, we can only determine the current density. This means that we can fix the current and only vary the number of windings of the magnet. As we feed the magnet with a current of $I = 75\text{ A}$ we choose this as our fixed value. For the number of windings we find a value of $N = 26853$. In order to keep a reasonable current density we also distribute the windings over four layers separated by 0.1 cm . This number might still be quite different to the actual amount, as real wires are expanded in space while we are working with wires represented by lines. For the radius we find a value of $R = 12.77\text{ cm}$ which is clearly larger than the bore radius but seems still reasonable considering isolation and the casing of the magnet. Also, the effective radius in the simulation is smaller due to the straight line approximation. The length proves to be about $L = 82.55\text{ cm}$ which might appear small compared to the casing length of 1 m but this value is closely constrained by the sharp edges in the magnetic field. Additionally, this potentially leaves space for some liquid helium and nitrogen vessels are necessary to surpass the critical temperature of the superconducting magnet. Additionally, as mentioned earlier, we include two shimming coils, one on each end. For each of them we predict $n = 1224$ windings, a radius of $r = 13.74\text{ cm}$ and a length of $l = 12.25\text{ cm}$ while using 2 layers of coils.

For the characterisation of the solenoid we did not use any additional coils but the code already includes the possibility to add any number of solenoid like shaped configurations. Ideally, this feature will even be manipulated so that one can angle and rotate the coil in space. In the current form we can only set an offset from the centre point of the solenoid.

With the Ben magnet we found different results which is to be expected with a different bore radius and case length. We still use a current of $I = 75\text{ A}$ but now find only $N = 16223$ windings at a radius of $R = 17.43\text{ cm}$. In comparison to the PSC the value for N seems reasonable due to a shorter length of $L = 52.64\text{ cm}$ and the radius also describes a similar distance to the casing. For the shimming coils we find $n = 2274$ which is almost double that of what we found for the PSC magnet. At the same time the length stays in the same regime with $l = 10.31\text{ cm}$. While we still use the same number of layers for this simulation, one could also repeat the simulation with more layers in order to further incorporate the winding to length ratio. For the radius we find a value of $r = 19.33\text{ cm}$

which is significantly larger than that of the main coil. One possible explanation for this could be the lack of further layers, which would need to be further investigated.

In addition to the named parameters, one will also find several normalisation parameters as well as global offset parameters for the position from the assumed measurement position. Introducing only a global offset and no individual offset for every position in the x-y-plane inevitably introduces an upper limit for the achievable accuracy of the simulation but is at the same time inevitable.

4.4 Systematic error patterns

Looking at some of the measurements of the PSC magnet in more detail we can clearly see a systematic error between different traces for a single measurement. We refer to a trace as measurements that were recorded after one another and are all set 10 cm apart. A measurement refers to all the data points that were recorded at the same x and y coordinates. These can therefore contain multiple traces, usually separated by 2 cm. The issue becomes much more clear by looking at the following two examples:

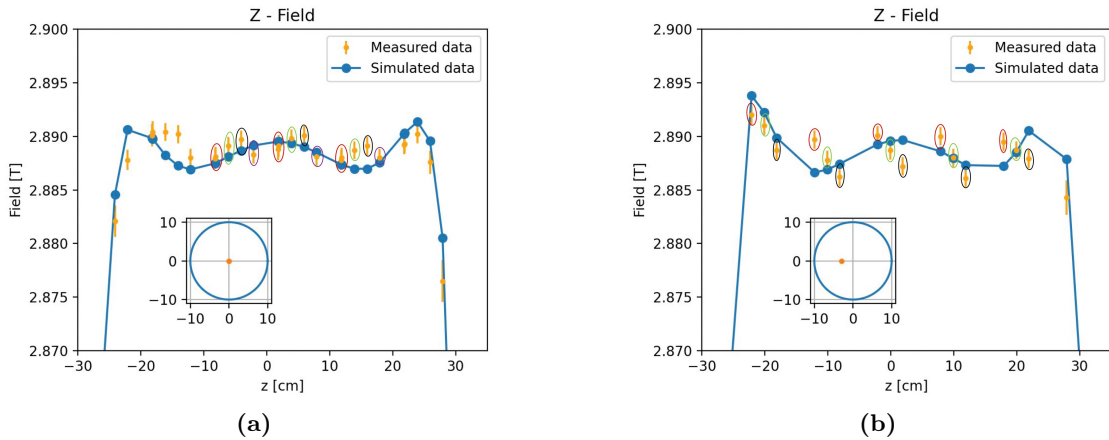


Figure 10: Z component of the magnetic filed around $z = 0$ for the center (10a) as well as $x = -30$ mm showing systematic measurement errors. Measurement points of the same trace are marked with the same colour. In figure 10a we see a repeated Γ like shape while in figure 10b we see a repeated line with a negative slope.

Without systematic errors we would expect the field to form a smooth surface similar to the one shown by the simulation. Instead we see repeating patterns within points of consecutive traces, leading to a correlation between the specific trace and the measurement point. For a good measurement we would only expect global and random errors and no correlation with the trace. Reasons for the occurrence of this phenomena could be slow fluctuations of the magnetic field, undetected external fields or a calibration offset of the probe which accumulates over time. One way to account for this error could be to include the uncertainty of reading and range in our overall uncertainty. These errors are given in the probes manual [8] as $\sigma_{range} = 0.005\% \cdot B_{max}$ and $\sigma_{reding} = 0.1\% \cdot B_i$. On the other

hand, as mentioned in section 2.2, we treated these errors to be time independent and therefore lead to an even offset over all measurement. The observation may therefore be the result of non-linear features of the probe as well as fluctuation in the field which we can not derive from our data and available information.

4.5 Direct comparison

While we have seen in the previous section that the precise field around the centre of the magnet is disturbed by systematic errors we still consider the results of our simulation in this region as valid and want to compare the results of the simulation for both magnets around the maximum field. When doing so we need to keep in mind that the limiting factor for both magnets on the maximum field was the range of the probe and the value was therefore set to 2.9 T when measuring. The PSC magnet can provide up to 5 T field in the center of the bore and the Ben magnet up to 4 T. We are therefore more interested in the shape of the field described by the magnets instead of the precise value of the magnetic field. The simulation results are shown in figure 11, which we will further discuss in the following.

The first notable difference is the length along the z axis over which we can observe a maximum field. Where the field of the PSC magnet covers about 60 cm the Ben magnet only reaches a maximum in a domain of about 20 cm. While large parts of this are clearly due to the difference in length of both magnets the effect is further enhanced by the larger radius of the Ben magnet. With a small radius, coils close to our point of interest have a much larger effect due to the inverse scaling in distance of the magnetic field. With larger radii coils become more and more equal. If we then increase distance to some part of the coils by leaving $z = 0$ there is less potential for compensation and the field falls off faster than that of a coil with smaller radii.

Furthermore, the PSC magnet shows local maxima at both ends of the magnet while there are non visible for the Ben magnet. This is in strong contrast to the data considered in section 4.2 where we did not zoom in on the data which meant that no peaks were visible for the PSC magnet around the same radius. On the other hand for the Ben magnet the outer measurement showed clear peaks, even without any zoom. This effect is due to the inverse scaling of the magnetic field in terms of the distance to the wire as well as the ratio between the length of the shimming coils and the length of the main solenoid. If the shimming coils are close to each other the fields will overlap around $z = 0$ and no of centre maxima will be visible. The local maxima in the centre of the PSC magnet is then the combination of the previously discussed effects where we have the maximum field of the main solenoid as well as the additional overlap of both side coils.

Additionally the PSC magnet also features a persistent mode [2]. In a persistent mode the magnet is first charged and then short-circuited with another piece of superconducting

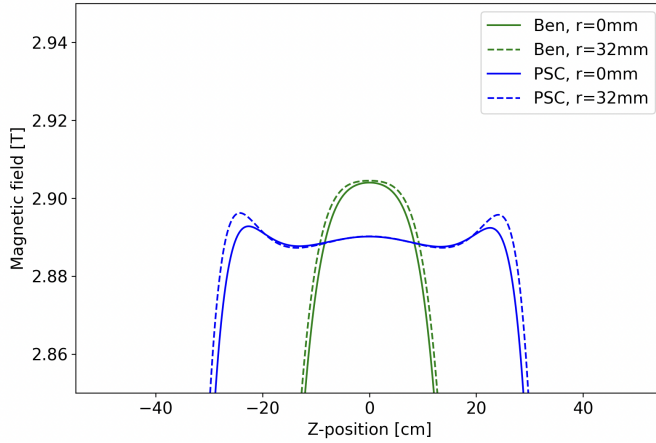


Figure 11: Close up view of the z component of the magnetic field around the maxima of both the Ben as well as the PSC magnet. For both magnets we show the simulation results at $r = 0\text{ mm}$ and $r = 32\text{ mm}$. The outer radius was chosen as it is of importance to the collaboration for the storage of the muons [2].

wire, leading to a near infinite loop of current. After the power supply is turned off the looping current stays much more stable than the current supplied by any power supply. This leads to a more stable field inside the magnet. A further discussion highlighting more characteristics of each magnet while translating these to the use and effect on the usability for the experiment can be found in the collaboration's proposal [2].

4.6 Information transfer for tracking simulations

As mentioned in the introduction our goal is to eventually run Monte Carlo simulations on injected muons. Such simulations rely on precise field maps as well as interpolation between data points in order to cover all possible positions in which we could find the particle. Using interpolation will inevitably lead to an error which we can minimise by using more precise field maps.

The tool we developed is able to create such field maps with up to micro meter precision. In order to reach such a high accuracy we needed to rewrite the code in such a way that only small amounts of data need to be stored in memory at the same time, essentially removing any memory bottlenecks due to memory overflow. In the package implementation this was the case as the field was simultaneously calculated for every field point. Here the limiting factor becomes the file size as it scales with an inverse cubic ratio meaning that if we half the spacing between two data points, the file size increases by a factor of eight. Even with millimetre spacing we reach file sizes of over 100 GB for the interior of the magnet. In order to avoid unnecessary data one can scale down the density in the less critical regions at the ends of the magnet but only dividing the step size by two in the centre would already reach the previous data size.

5 Conclusion and Outlook

Over the course of this thesis we were able to create a powerful tool to calculate the magnetic field data for arbitrary wire configurations. In order to generate any configuration we establish a fundamental element as a small straight piece of wire which is then used to approximately build shapes such as circles and solenoids. Within the scope of this project we used this to fit parameters of a solenoid to the data recorded within two solenoids at PSI. While the tool initially relied on a public python package named `Biot-savart` [9] we adjusted most aspects of the package, most importantly did we change the calculation of a straight piece of wire so that it is based on the analytical solution of Biot Savart's law. Additionally we were able to structure the code in such a way that allowed us to perform several evaluations per second, even for large data sets and relatively fine configurations. This allowed us to run global optimisations on many, relatively unknown, parameters over short periods of time. From this we generated field data which not only closely recreates the measured data but was also far more accurate than the initial fits using commercial software.

While we were able to keep errors which are introduced by any approximations within the model small, we observed a limiting factors for accuracy in clear systematic errors from the measurement data. In order to improve the evaluation process we used weight rescaling of the data points in accordance to a uncertainty model.

From the results we are now able to export the fields inside the magnets to different platforms in order to perform Monte Carlo simulations on position and spin tracking. Once we are able to resolve the question of the necessary accuracy of the field map, the results will give us valuable insight for a potential muon EDM measurement at PSI and help us decide the between one of the two available magnets.

After the initial simulations with the current configurations the implementation will further enable us to calculate the field introduced by additional devices which are necessary for the execution of the experiment. For this we do not only include parts that conserve the cylindrical symmetry of the system but principle anything that we can recreate using small pieces of straight wire.

Acknowledgement

First of all I would like to thank Prof. Dr. Klaus Kirch for giving me the opportunity to contribute to the exciting collaboration. Here I would also like to thank Dr. Philipp Schmidt-Wellenburger as the spokesperson of the muon EDM collaboration at PSI for allowing me to present my findings to the entire collaboration as well as the valuable input I received when discussing the current state of my project.

I want to give special thanks to my supervisor Dr. Chavdar Dustov for the continuous guidance throughout the project with a lot of helpful discussions and skills that will help me going far beyond this project. Without the continues support I could not have enjoyed and concluded the project the way that I did.

Lastly I would like to thank Anastasia and Tim as well as all the other members of the collaborations around us at PSI for making this a very fun and exciting experience.

References

- [1] G. W. Bennett et al. (Muon (g-2) Collaboration), *Improved limit on the muon electric dipole moment*, Phys. Rev. D 80, 052008 – Published 21 September 2009, <https://doi.org/10.1103/PhysRevD.80.052008>
- [2] P. Schmidt-Wellenburg et al. (Muon EDM Collaboration), *Measurement of the Muon Electric Dipole Moment*, PSI Proposal No. R-21-02.1, January 2023
- [3] Klaus Jungmann, *Searching for electric dipole moments*, Review Article Ann. Phys. (Berlin) 525, No. 8–9, 550–564 (2013), <https://doi.org/10.1002/andp.201300071>
- [4] A. Crivellin, M. Hoferichter, P. Schmidt-Wellenburg, *Combined explanations of $(g - 2)_{\mu,e}$ and implications for a large muon EDM*, Phys. Rev. D 98, 113002 – Published 7 December 2018, <https://doi.org/10.1103/PhysRevD.98.113002>
- [5] F. J. M. Farley et al., *New Method of Measuring Electric Dipole Moments in Storage Rings*, Phys. Rev. Lett. 93, 052001 – Published 27 July 2004, <https://doi.org/10.1103/PhysRevLett.93.052001>
- [6] C. Dutsov, T. Hume, P. Schmidt-Wellenburg, *Systematic effects in the search for the muon electric dipole moment using the frozen-spin technique*, (November 2022), <https://doi.org/10.48550/arXiv.2211.13506>
- [7] Tsz Leung Tang (July 10, 2021), *Finite length Solenoid potential and field*, <https://nukephysik101.files.wordpress.com/2021/07/finite-length-solenoid-potential-and-field-1.pdf> [accessed 26.01.2023]

- [8] Product page of *Model 460 3-Channel Gaussmeter*, <https://www.lakeshore.com/products/categories/overview/discontinued-products/discontinued-products/model-460-3-channel-gaussmeter> [accessed 31.01.2023]
- [9] M. Yin, R. Zazo, PyPi page of *biot-savart* python package, <https://pypi.org/project/biot-savart/> [accessed 03.04.2023]
- [10] M. Newville et al., GitHub page for *lmfit* python package, <https://lmfit.github.io/lmfit-py/index.html> [accessed 03.04.2023]

Appendices

Python-code

A current version of the code is available under the following git repository:

https://github.com/ppestlin/BT_magnetic_field_optimization

The repository might be subject to change after the conclusion of this thesis for further improvements or additional functionality. In order to run the code the installation of several, commonly used packages is necessary. For access to the measurement data please reach out.

Additional graphics

Here we show additional graphics which were not yet shown in the previous sections.

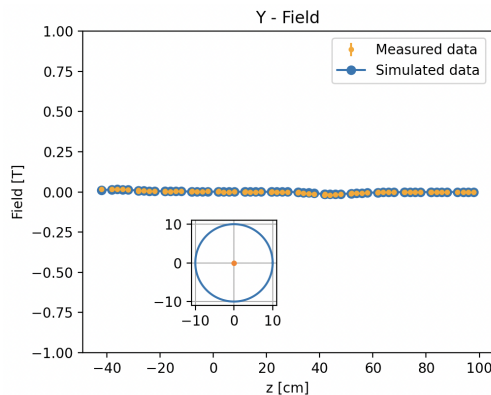


Figure 12: PSC Y-Field in the center

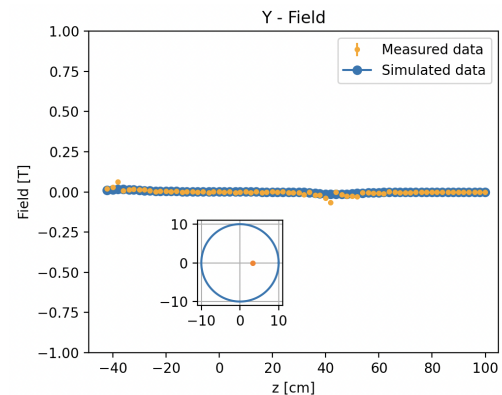


Figure 13: PSC Y-Field at $x = 3.3\text{cm}$

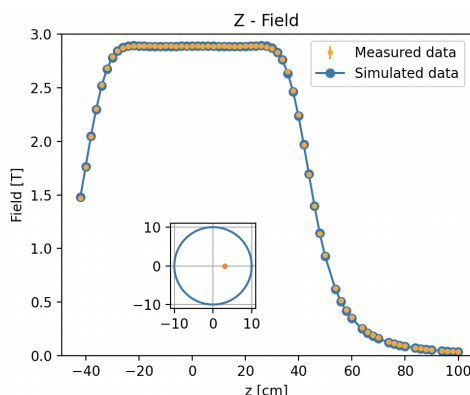


Figure 14: PSC Z-Field at $x = 3.0\text{ cm}$

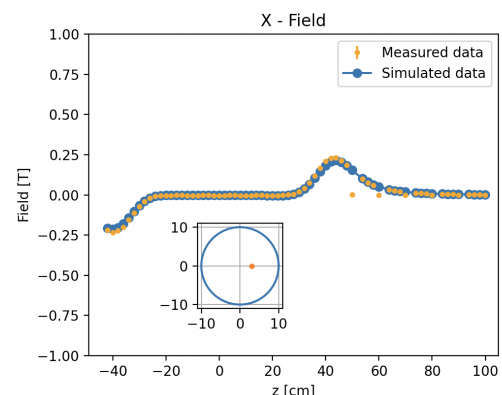


Figure 15: PSC X-Field at $x = 3.0\text{ cm}$

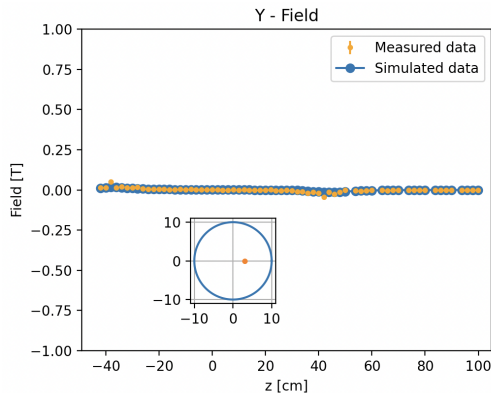


Figure 16: PSC Y-Field at $x = 3.0$ cm

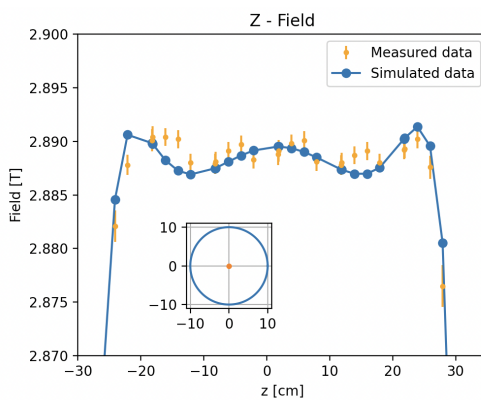


Figure 17: PSC Z-Field in the center, without markers (see figure 10a)

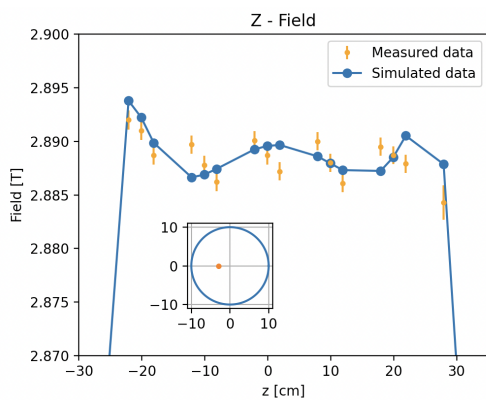


Figure 18: PSC Z-Field at $x = 3.0$ cm, without markers (see figure 10b)

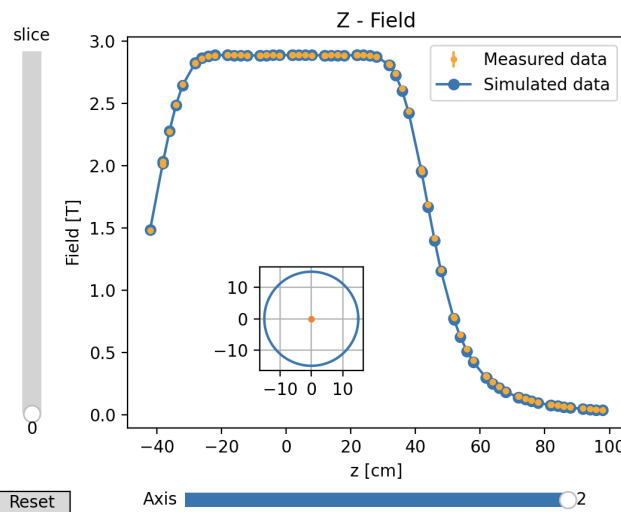


Figure 19: Overview of the plotted interface from which all similar plots were created. The two sliders can be used to access different axes or the other field components. In order to zoom in, one can use the native matplotlib tools

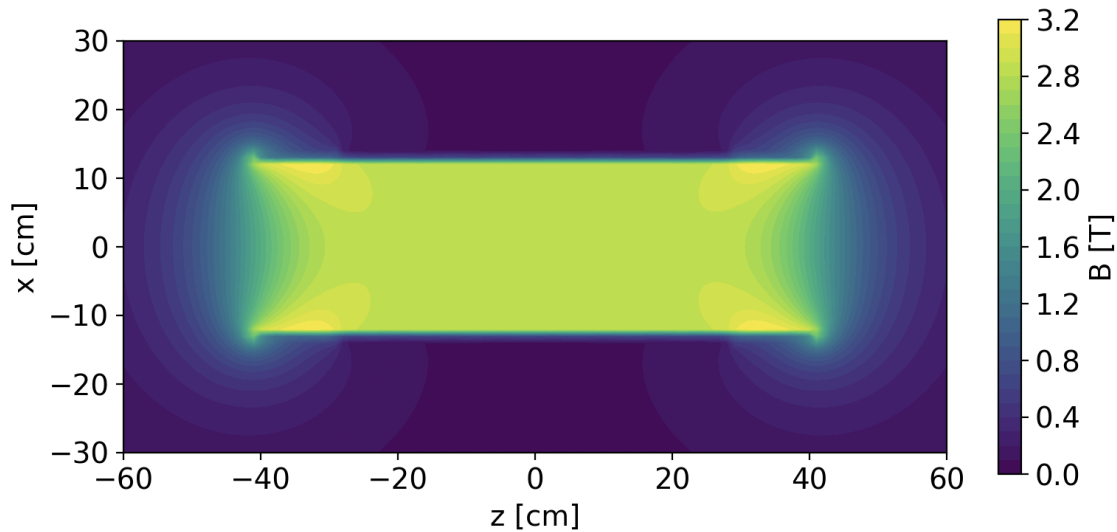


Figure 20: Contour plot of the PSC magnet without indicated boundaries (see figure 6)

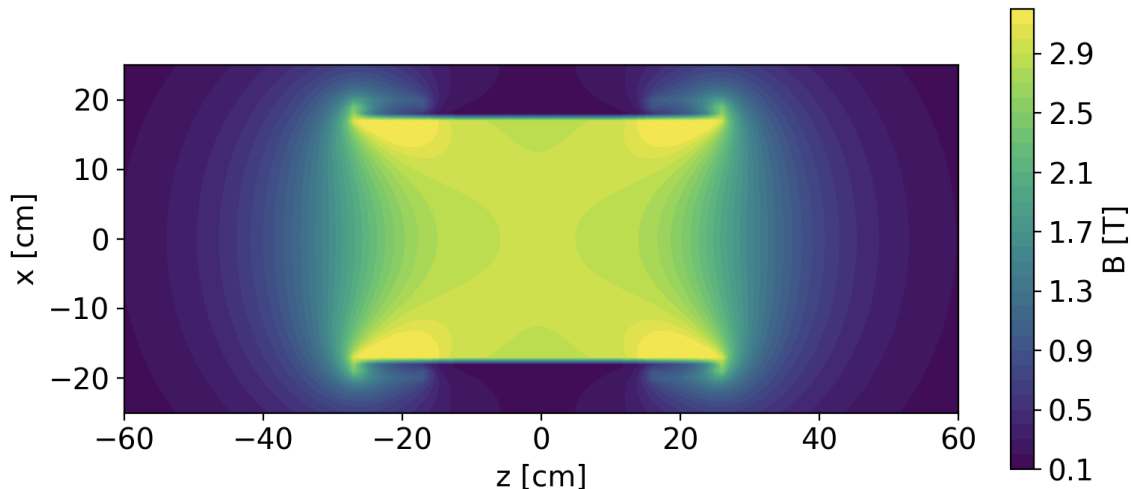


Figure 21: Contour plot of the Ben magnet without indicated boundaries (see figure 9)

Declaration of originality

The signed declaration of originality is a component of every semester paper, Bachelor's thesis, Master's thesis and any other degree paper undertaken during the course of studies, including the respective electronic versions.

Lecturers may also require a declaration of originality for other written papers compiled for their courses.

I hereby confirm that I am the sole author of the written work here enclosed and that I have compiled it in my own words. Parts excepted are corrections of form and content by the supervisor.

Title of work (in block letters):

Authored by (in block letters):

For papers written by groups the names of all authors are required.

Name(s):

First name(s):

With my signature I confirm that

- I have committed none of the forms of plagiarism described in the '[Citation etiquette](#)' information sheet.
- I have documented all methods, data and processes truthfully.
- I have not manipulated any data.
- I have mentioned all persons who were significant facilitators of the work.

I am aware that the work may be screened electronically for plagiarism.

Place, date

Signature(s)

Peblin

For papers written by groups the names of all authors are required. Their signatures collectively guarantee the entire content of the written paper.